Cocrystallization-like strategy for the codelivery of hydrophobic and hydrophilic drugs in a single carrier-free formulation

Yi Li[1], Chao Teng[1], Helena S Azevedo[2], Lifang Yin[1], Wei He[1,*]

[1] School of Pharmacy, China Pharmaceutical University, Nanjing 210009, China

[2] School of Engineering and Materials Science, Institute of Bioengineering, University of London, London E1 4NS, UK

[*]Corresponding author.

E-mail address: weihe@cpu.edu.cn (Wei He).

Abstract

Codelivery of drugs is a promising strategy against several diseases such as infections and cancer. However, traditional drug carriers are typically characterized by having low drug payload limiting their long-term treatment efficacy. Using nanocrystals of insoluble drug as carriers, a carrier-free platform was developed previously to deliver a second insoluble drug for codelivery. To extend the concept, we hypothesized, herein, that the platform allows for codelivery of hydrophobic and hydrophilic drugs using a cocrystalization-like strategy. To obtain proof-of-concept, an insoluble chemotherapeutic agent, paclitaxel (PTX), and a water-soluble inhibitor of pyruvate dehydrogenase kinase, dichloroacetic acid (DCA), were utilized as model drugs. PTX-DCA hybrid nanocrystals (PTX-DCA NCs) were prepared by anti-solvent precipitation and characterized. Their *in vitro* antitumor activity against cancer cells was evaluated. PTX-DCA Ns prepared from the optimized formulation had a diameter of 160 nm and a rod-shape morphology and possessed encapsulated efficacy of approximately 30% for DCA. The use of the hybrid crystals enabled synergy to kill cancer cells, in particular in PTX-resistant cells in a dose-dependent pattern. In conclusion, by using a cocrystalization-like strategy a hydrophilic drug can be formulated into in a drug's nanocrystals for codelivery.

Keywords: hybrid nanocrystal; codelivery; multidrug resistance; paclitaxel; DCA; cocrystallization

Introduction

Codelivery of two drugs or more is a promising approach for combinatory therapy and treating diseases, due to its benefits such as enhanced therapeutic selectivity, synergy, reduced side effects, and improved patient's compliance [1]. Drug-carrier techniques, encompassing liposomes, polymeric micelles, nanoemulsions, solid lipid nanoparticles, carbon nanotubes, and inorganic particles are commonly used to facilitate drug delivery [2-5]. However, these drug carriers often have low drug-loading capacity, typically less than <10% (w/w) and, as a result, limiting the treatment efficacy [6-8]. Furthermore, the low payload becomes more restrictive in codelivery as multiple drugs are required for loading.

Nanocrystals of insoluble active compounds are nanoscale drug particles [9, 10]. Nanocrystals have noticeably high drug-loading since the nanocrystal particles are 100% drug[10, 11]. Previously, by using drug nanocrystals as carriers, a carrier-free platform of codelivery was developed to codeliver insoluble drugs [12, 13]. We demonstrated that via a cocrystalization-like strategy one drug could be incorporated into the second drug's nanocrystals, forming hybrid drug crystals to improve delivery of the two hydrophobic drugs [12, 13]. Herein, we hypothesized that the cocrystalization approach allows codelivery of insoluble and hydrophilic drugs as well, which the water-soluble drug is formulated inside the crystals of hydrophobic drug.

Paclitaxel (PTX) is a poorly water-soluble chemotherapeutic drug with a water solubility of 0.3 mg/mL [14]. PTX is potent to kill cancer cells and acts via destroying the dynamic balance between tubulin and tubulin dimer, and as a result, inhibiting the mitosis of cancer cells and inducing apoptosis [15]. On the other hand, dichloroacetic acid (DCA), a small molecule inhibitor of pyruvate dehydrogenase kinase, enables promoted apoptosis by interfering with glucose metabolism in cancer cells [16]. Recent studies demonstrated that DCA could inhibit stress cell autophagy [17, 18] and reverse multi-drug resistance（MDR) by reducing the activity of drug efflux pump on cell membrane [19]. Besides, DCA is also reported to have the function of switching cytoplasmic glucose metabolism to mitochondrial oxidative phosphorylation [20, 21]. As a result, DCA has potential to increase the sensitivity of drug-resistant cancer cells to PTX.

To obtain proof-of-concept, we prepared and characterized PTX-DCA hybrid nanocrystals (PTX-DCA Ns) (Figure 1). Furthermore, to demonstrate potential treatment efficacy, their *in vitro* antitumor activity against PTX-resistant cancer cells, A549/TAX cells, was evaluated.

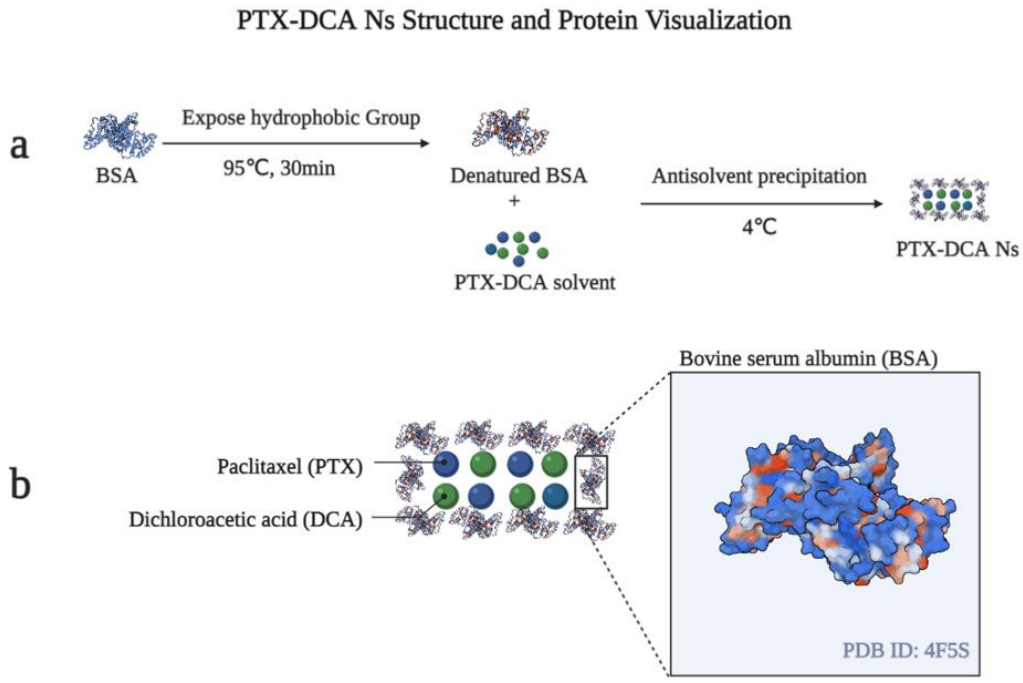

Figure 1 Scheme illustrating the preparation of PTX-DCA Ns via anti-solvent precipitation (a) and PTX-DCA NCs stabilized with BSA (b).

Materials and Methods

Materials

Paclitaxel (99% purity) was purchased from Jiangsu Yew Biotechnology, China. DCA (99% purity), bovine serum albumin (BSA) and 3-(4, 5-dimethylthiazol-2-yl)-2, 5-diphenyltetrazolium bromide (MTT) were obtained from Sigma-Aldrich, USA. Annexin V-FITC/PI Apoptosis Detection Kits, phosphate-buffered saline (PBS), penicillin, streptomycin, trypsin-EDTA (> 6000 U/mg), and the adenocarcinomic human alveolar basal epithelial cell line A549 were purchased from Nanjing KeyGen Biotechnology, China.

Preparation and characterization of hybrid drug nanocrystals

PTX-DCA NCs were prepared by an anti-solvent precipitation process and using denatured BSA as stabilizer. In brief, BSA was dissolved in distilled water to obtain a concentration of 1 mg/mL, followed by adjusting pH to 7.0, stirring for 2 hours at room temperature, heating at 95 °C for 30 min, and then cooling to 4 °C before use [22]. Briefly, 10 mg of PTX was dissolved in 1 mL of acetone and mixed with 2 mg of DCA. The organic solution was added dropwise to 10 mL of pre-chilled BSA solution under constant stirring. After the precipitation process, the mixture was

immediately moved to an ice-bath and subjected to periodic 3-s ultrasonication at 20-25 kHz and 250 W for 15 min, with 4-s intervals. Finally, the nascent sample was evaporated under reduced pressure, filtered through a 0.22-μm hydrophilic polyvinylidene fluoride membrane (Millipore, USA), and stored at 4 °C for further use.

Particle size and polydispersity index (PDI)

The particle size and PDI of PTX-DCA NCs were measured on a NanoBrook 90Plus Zeta Plus Zeta Potential Analyzer (Brookhaven Instruments, USA). Measurements were performed at 25 °C over 5 min, at an angle of 90°. The size of the nanoparticles was expressed as an intensity-weighted Gaussian distribution ($Chi^2 < 3$).

Transmission electron microscopy (TEM)

Structural characterization of PTX-DCA Ns was conducted on a JEM-1230 Transmission Electron Microscope (JEOL, Japan) at an accelerating voltage of 200 kV. Specifically, the preparation was diluted 200-fold and 25 μL of the dilution was placed onto the copper mesh and dried at 20 °C for 30 min. After removing excess sample with filter paper, the sample was stained for 30 s by adding a drop of 2% (w/w) phosphotungstic acid. The superfluous phosphotungstic acid was carefully removed and the stained sample was desiccated at 25 °C for 5 min.

In vitro stability

PTX-DCA NCs were resuspended in a PBS solution with 10% fetal bovine serum (FBS) at pH 7.4 at 37 °C. The *in vitro* stability of the resultant suspension was evaluated by measuring particle size and PDI every 2 h for a period of 12 h based on aforementioned experimental procedures.

Powder X-ray diffraction (PXRD) analysis

PXRD analysis was performed on a D8 ADVANCE X-Ray Powder Diffractometer (Bruker, Germany) using a copper anode with tube voltage at 40 kV, current at 60 mA and λ (Cu Kα) at 0.154 nm. Data was acquired under step-scan mode in the 2θ range of 2.5 to 50° at a scanning rate of 3° per min and a step increment of 0.02°.

Fluorescence and circular dichroism (CD) spectroscopy

Fluorescence spectroscopic studies were performed on a RF-5301PC fluorescence spectrometer (Shimadzu, Japan) in the wavelength range of 300 to 800 nm, with the excitation wavelength set to 295 nm. CD spectroscopic studies were performed at 25 °C on a J-810 Circular Dichroism Spectropolarimeter (JASCO, Japan) in the wavelength range of 190 to 420 nm (far: 190 to 250 nm; near 250 to 420 nm) at a scan rate of 100 nm/min. Ellipticity was expressed in millidegrees. The bandwidth, response time and cell size were set to 1 nm, 1 s and 0.1 cm, respectively.

Encapsulation efficiency (EE%)

Briefly, 5 mL of the sample were centrifuged at 10,000 g and 4 °C. The supernatant was immediately discarded, and the pelleted viscous white precipitate was re-dissolved in 10 mL of

methanol, the pH of which was pre-adjusted to 2.0 with phosphoric acid. Subsequently, 20 μL of the methanol solution was injected into an LC-10AT high-performance liquid chromatography (HPLC) system (Shimadzu, Japan) equipped with a Diamonsil C18 octadecylsilane-bonded silica gel column (4.8 mm × 200 mm, 5 mm; Dikma Technologies, USA). Separation was performed at 25 °C by using a mobile phase consisting of 80% methanol, 10% acetonitrile and 10% water (v/v), pre-adjusted to pH 2.0 with phosphoric acid, at a constant flow rate of 1 mL/min. The detection of DCA was performed at 214 nm. The EE% of DCA was calculated using the formula below:

EE% = Amount of encapsulated DCA/Amount of added DCA × 100%

Establishment of the paclitaxel resistant A549/TAX cell line

The PTX-resistant A549/TAX cell line was prepared by exposing A549 cells to increasing concentrations of PTX, as previously described [23]. Briefly, A549 cells in logarithmic growth phase were first cultured for 48 h in RPMI 1640 medium supplemented with 10% FBS and 100 μg/mL streptomycin at 37 °C and under a humidified atmosphere of 5% CO_2. After reaching 80% confluence, the cells were collected, resuspended in a fresh RPMI 1640 medium containing 20 ng/mL PTX and cultured for 24 h. The surviving cells were harvested and recovered in PTX-free RPMI 1640 medium until the next logarithmic phase. The two-stage treatment cycle was repeated with a progressively higher concentration of PTX (20, 40, 60, 80, 100, 200, 300 and 400 ng/mL), until the cells showed steady growth in the presence of 400 ng/mL PTX. The drug resistance of the resultant A549/TAX cells was maintained in culture medium containing 100 ng/mL of PTX. Prior to use, the cells were cultivated in PTX-free medium for at least 3 days.

Cytotoxicity and synergy

The cytotoxicity of different drug formulations in A549 and A549/TAX cells was measured by the MTT assay. Briefly, the cells were seeded in a 96-well plate at a density of 5×10^4 cells per well, cultured with diluted preparations for 24 h at 37 °C, incubated with 20 μL of 5 mg/mL MTT for another 4 h, and 150 μL of DMSO. The absorbance was measured on a Multiskan FC Microplate Photometer (Thermo Fisher Scientific, USA) at 490 nm. IC_{50} was calculated using Prism software (version 5.01; GraphPad, USA).

The synergy between PTX and DCA was calculated by using the CI and DRI equation described below.

$$CI = D_1 / D_{x1} + D_2 / D_{x2}$$

$$DRI_1 = D_{x1} / D_1$$

where D_{x1} and D_{x2} denote the IC_{50} of PTX and DCA in the standalone treatment, respectively. D_1 and D_2 correspond to the IC_{50} of PTX and DCA in the combination treatment, respectively. CI <1, CI = 1 and CI > 1 represent synergistic, additive and antagonistic effects, respectively. CompuSyn 1.0 software (ComboSyn, Inc., USA) was used for computing CI and DRI.

Cell apoptosis

Cells were first seeded in a 6-well plate at a density of 5×10^5 cells per well and treated at 37 °C for 24 h with various dilutions of different drug formulations. The cells were subsequently collected, washed with PBS three times, stained at room temperature for 15 min using an Annexin V-FITC/PI Apoptosis Detection Kit, and analyzed on an Accuri C6 Plus flow cytometer (BD, USA).

Statistical analysis

All quantitative experiments were performed in triplicate. Data were expressed as mean ± standard error. Differences between two experimental groups were evaluated by the Student's t-test. $P < 0.05$ was considered statistically significant.

Results and discussion

Preparation and characterization

We first prepared the hydrid nanocrystals PTX-DCA NCs via anti-solvent precipitation with denatured BSA as a stabilizer. To optimize the formulations, we tested the influence of ultrasonication conditions on the particle size, PDI and EE% of the resultant nanocrystals. Dynamic light scattering measurements indicated that both the average particle size and PDI first declined, but then increased, with prolonged ultrasonic treatment and increase of energy intensity (Figure 2a). This trend reversal suggested that prolonged ultrasonication with excessive power-input could potentially disrupt the nanocrystal structure and lead to aggregation of PTX-DCA NCs. HPLC assay showed an inverse correlation between the EE% of DCA with the promoted ultrasonic treatment (Figure 2d). As a result, the nanocrystal preparations were conducted at a power intensity of 250 W for a duration of 15 min.

We next examined the effects of PTX-DCA mass ratio on the nanocrystal formation by fixing the amount of PTX at 10 mg and varying DCA from 2 to 10 mg with 2-mg increment. The average particle size of PTX-DCA NCs declined first and then rose with the reduced ratio (Figure 2b), whereas the EE% of DCA exhibited a steady decrease, as the mass ratio increased (Figure 2e). Therefore, the optimal mass ratio of PTX to DCA of 5: 1 was selected for next study (10 mg PTX and 2 mg DCA).

Further optimization was focused on the evaluation of different drug payload levels under the ultrasonication conditions and mass ratio specified above. The elevation of the drug payload from 1 mg to 30 mg (based on PTX) led to an increase in both particle size and PDI (Figure 2c), but a drop in EE% (Figure 2f). Accordingly, the mass ratio of 10 mg of PTX and 2 mg of DCA in PTX-DCA NCs was optimized drug loading.

Taken together, we concluded that the optimal protocol for preparing PTX-DCA NCs is as follows: performing ultrasonic treatment on the formulation of 10 mg of PTX and 2 mg of DCA at a power intensity of 250 W for 15 min. Under these conditions, the average diameter and PDI of the nanoparticles were measured to be 160.48 nm and 0.153, respectively (Figure 2g). TEM characterization revealed the nanocrystals have a rod shape with a typical particle size around 160 nm (Figure 2h), consistent with the results from dynamic light scattering data.

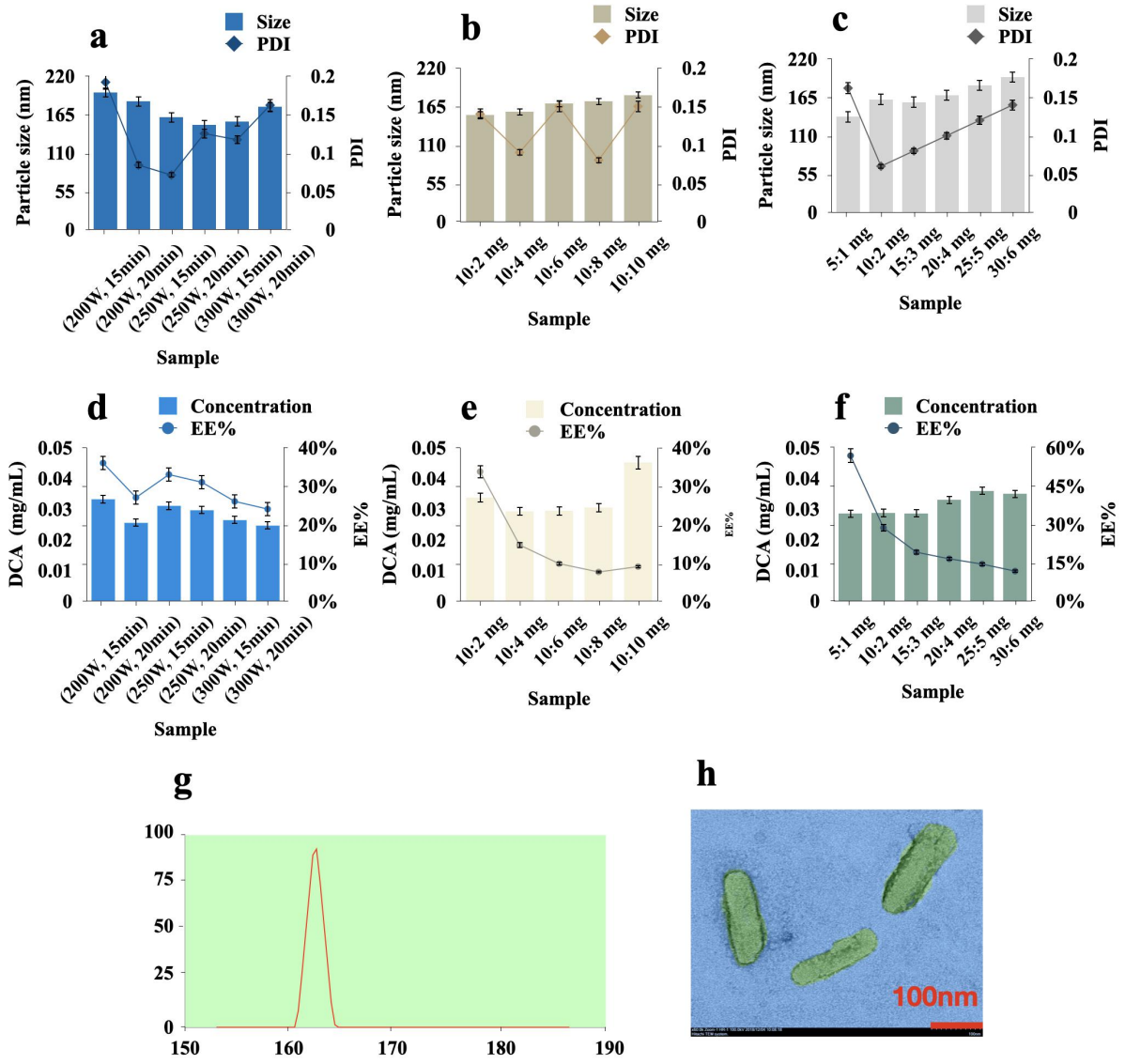

Figure 2 Preparation and characterization of the hybrid drug NCs. (a-c) average particle size and PDI, (d-f) EE% of DCA in various formulations of PTX-DCA NCs. (c) Average particle and PDI and (d) the EE% of DCA in the prepared PTX-DCA NCs with different mass ratios of PTX to DCA. (e) Average particle and PDI and (f) the EE% of DCA of the prepared PTX-DCA NCs at different drug payloads. (g) Size distribution and (h) TEM image of PTX-DCA NCs prepared from the optimized formulation, involving the use of 10 mg of PTX and 2 mg of DCA, subjected to ultrasonic treatment at a power intensity of 250 W for 15 min.

In vitro stability and PXRD analysis

Serum stability was performed by incubating the nanoparticles in PBS containing 10% FBS. One-hour incubation resulted in approximately 20-nm growth of the nanoparticles due to the adsorption of serum proteins, whereas no significant variation was observed in the diameter 1 h later (Figure 3a), suggesting their potential stability after intravenous administration.

PXRD analysis shows crystalline PTX has a well-defined characterized peak at 2θ = 5.54°, 9.12° and 12.54° (Figure 3b). The PTX-BSA mixture displays similar peaks to the pure PTX, and amorphous BSA producing no diffraction peaks (Figure 3b). Interestingly, PTX-DCA NCs with

low payload (2 mg of DCA and 10 mg of paclitaxel) exhibited an amorphous state with no defined diffraction peaks, whereas those with a 5-fold increase of payload displayed two characteristic signals at 5.44°and 12.62°. These results confirmed that the nanoparticles are mainly present as microcrystals

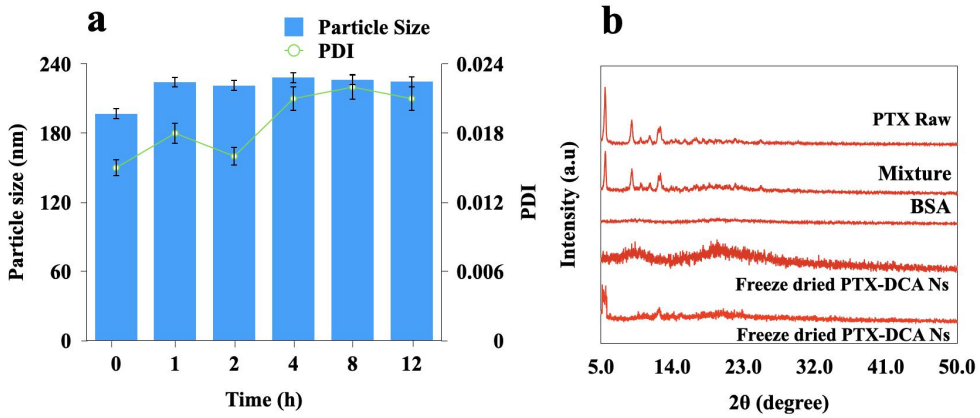

Figure 3 (a) *In vitro* stability of the NCs after incubation in serum-containing PBS; . (b) PXRD characterization.

Fluorescence and CD characterization

The fluorescence emission spectra of native BSA in PBS solution registered a characteristic broad band at 340 nm attributable to tryptophan residues [24]. The intensity of this band was found to decline significantly in denatured BSA (Figure 4a). In the presence of PTX-DCA NCs, we observed a clear inverse correlation between the signal intensity of the 340-nm band and the drug payload (Figure 4b), which might be due to fluorescence quenching of the tryptophan residues in BSA following its binding to the highly polar DCA in the nanocrystals. Curve fitting of the fluorescence data based on the Stern-Volmer equation [25] suggested that DCA led to the static fluorescence quenching of BSA and the two were connected by strong interaction ($y = 0.9604x + 0.2738$, $r = 0.9956$; Figure 4c). These experimental data confirmed that the the hybrid crystals could interact with BSA and modulate its environment in a dose-dependent manner.

The conformational changes of BSA after interacting with hybrid crystals were further investigated by far- and near-UV CD spectra [26]. The spectrum of denatured BSA shows a narrow peak at 195 nm that could be attributed to its α-helices, and a broad band at 235 nm that might arise from the conversion of the α-helices to β-folds (Figure 4d), leading to enhanced structural stability of the protein [27]. However, few characterized peaks are observed in the near-UV spectrum (Figure 4e). This broad band in the far-UV spectrum showed a significant red-shift in the presence of hybrid crystals (Figure 4f), probably indicating the exposure of the tryptophan residues in BSA [28]. In addition, the 235-nm band was more intense with an increase of drug payloads, suggesting a concentration-dependent structural alteration of crystal-bound BSA. In the near-UV spectrum, fluorescence amplification at wavelengths of around 260 and 290 nm for the addition of the hybrid crystals is observed as well (Figure 4g). Compared to native BSA, the structure of denatured BSA detected in this band does not have typical circular dichroism; while the preparation has a positive peak at 260 nm and a negative peak at 290 nm, respectively, corresponding to the β-angle and random coil structure, which may be due to the combination of protein residues and heteroatoms, resulting in its optical activity. Taken together, the observed payload-dependent conformational changes of BSA in the presence of hybrid crystals identified the interaction between the protein and the crystals and proved that the denatured BSA could serve as a stabilizer for the nanocrystals [29].

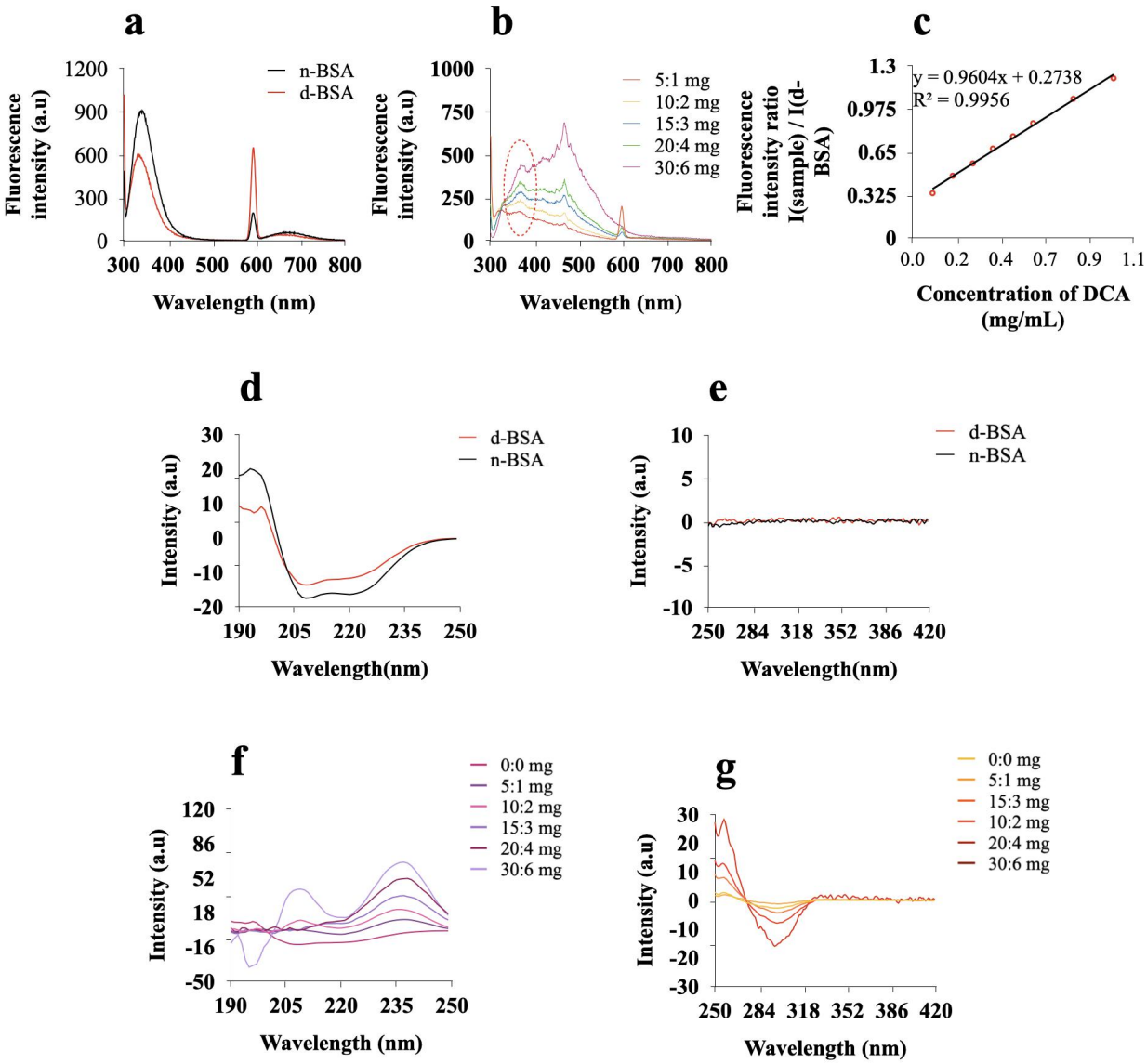

Figure 4 Fluorescence spectra of (a) BSA and (b) PTX-DCA NCs at different drug payloads. (c) Data fitting based on the Stern Volmer equation. CD spectra of native and denatured BSA in the wavelength range of (f) 190 to 250 nm (far UV) and (d) 250 to 420 nm (near UV). CD spectra of PTX-DCA NCs at different drug payloads in the wavelength range of (g) 190 to 250 nm (far UV) and (e) 250 to 420 nm (near UV). The aqueous concentration of BSA was 1.0 mg/mL for the fluorescence spectroscopy and 0.5 mg/mL for the CD characterization.

Cytotoxicity and synergistic effects

As depicted in Figure 5 (a and b), all preparations exhibited dose-dependent cytotoxicity to both A549 and A549/TAX cells. Treatment with PTX-DCA NCs allowed for enhanced toxicity against the cancer cells over the incubation with one drug alone. Compared with free-drug combination, PTX-DCA NCs have generally improved cytotoxicity due to promoted cellular uptake. Especially, the combinatorial formulations, PTX-DCA NCs and free-drug combination, demonstrated higher toxicity to the PTX-resistant cells, A549/TAX cells, over A549 cells at the doses of 50 and 100 μg/mL. These results indicated that DCA is able to increase the sensitivity of cancer cells, in particular the drug-resistant cells, to the chemotherapeutic drug PTX.

To evaluate the synergy between PTX and DCA, the combination index (CI) and dose reduction index (DRI) were calculated at IC_{50} according to the cytotoxicity. As depicted in Figure 5 (c and d), all determined CI are less than 1, indicating the synergistic effects. Also, the CI values from other ICs are lower than 1 and further demonstrated the rationality to combinatorically use the two drugs. Furthermore, the DRIs of PTX-DCA NCs for the two cell lines are greater than that from the free-drug combination (Figure 5, e and f). Particularly, PTX-DCA NCs displayed improved increment of DRI for the drug-resistant cells over that for A549 cells. In addition, the CIs from IC_{50}, IC_{65}, IC_{75}, and IC_{90} in the drug-resistant cells are less than that in A549 cells.

To further study the anti-tumor activity *in vitro*, examination of apoptosis in A549 cells and A549/TAX cells was performed. The free-drug combination induced apoptosis with higher efficacy than PTX or DCA alone (Fig. 6). Importantly, PTX-DCA NCs demonstrated promoted ability to kill the cancer cells over the free-drug combination. Again, PTX-DCA NCs exhibited improved potency to induce apoptosis in the drug-resistant cells over A549 cells. These results indicated that PTX and DCA have synergistic effect to kill cancer cells, especially PTX-resistant cells, and formulating them into hybrid crystals confers improved synergy.

Conclusion

In this study, we demonstrated that via a cocrystalization-like approach a hydrophilic drug can be loaded into nanocrystals of an insoluble drug and form hybrid crystals for codelivery. Our previous reports revealed that the cocrystalization-like strategy facilitated codelivery of two insoluble drugs [12, 13]. Overall, the nanocrystals of a hydrophobic drug are effective to encapsulate both hydrophobic and hydrophilic active compounds acting as promising “carriers” for codelivery considering their extremely high drug-loading ability. Using the present platform, codelivery of PTX and DCA demonstrated synergy in killing cancer cells, especially PTX-resistant cells.

Acknowledgment

This study was supported by the National Natural Science Foundation of China (Nos. 81872823, 81673377 and 82073782), the Double First-Class (CPU2018PZQ13, China) of the China Pharmaceutical University, the Shanghai Science and Technology Committee (No. 19430741500), and the Key Laboratory of Modern Chinese Medicine Preparation of Ministry of Education of Jiangxi University of Traditional Chinese Medicine (TCM-201905, China).

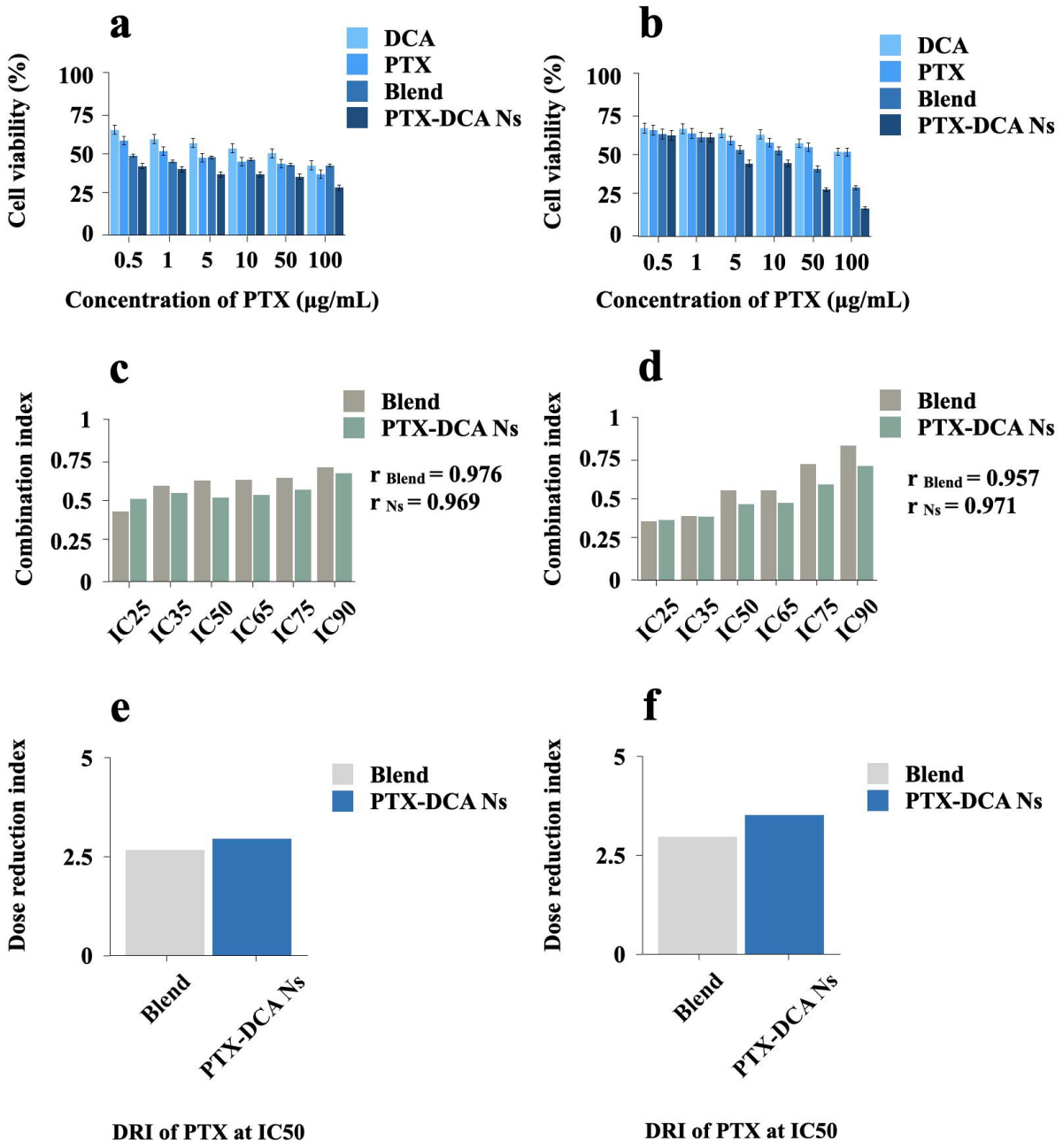

Figure 5 Cell viability and drug synergy effects. (a) A549 cells or (b) A549/TAX cells were incubated with preparations for 24 h at 37 °C. The mass ratio for PTX to DCA in the combination and the nanocrystal formulations was 5: 1. CI values of the combination and PTX-DCA NCs in (c) A549 and (d) A549/TAX cells. Dose reduction index (DRI) values for PTX in (e) A549 or (f) A549/TAX cells. IC values were calculated according to PTX concentration. CI <1, CI =1 and CI >1 indicate synergistic, additive, and antagonistic effects, respectively.

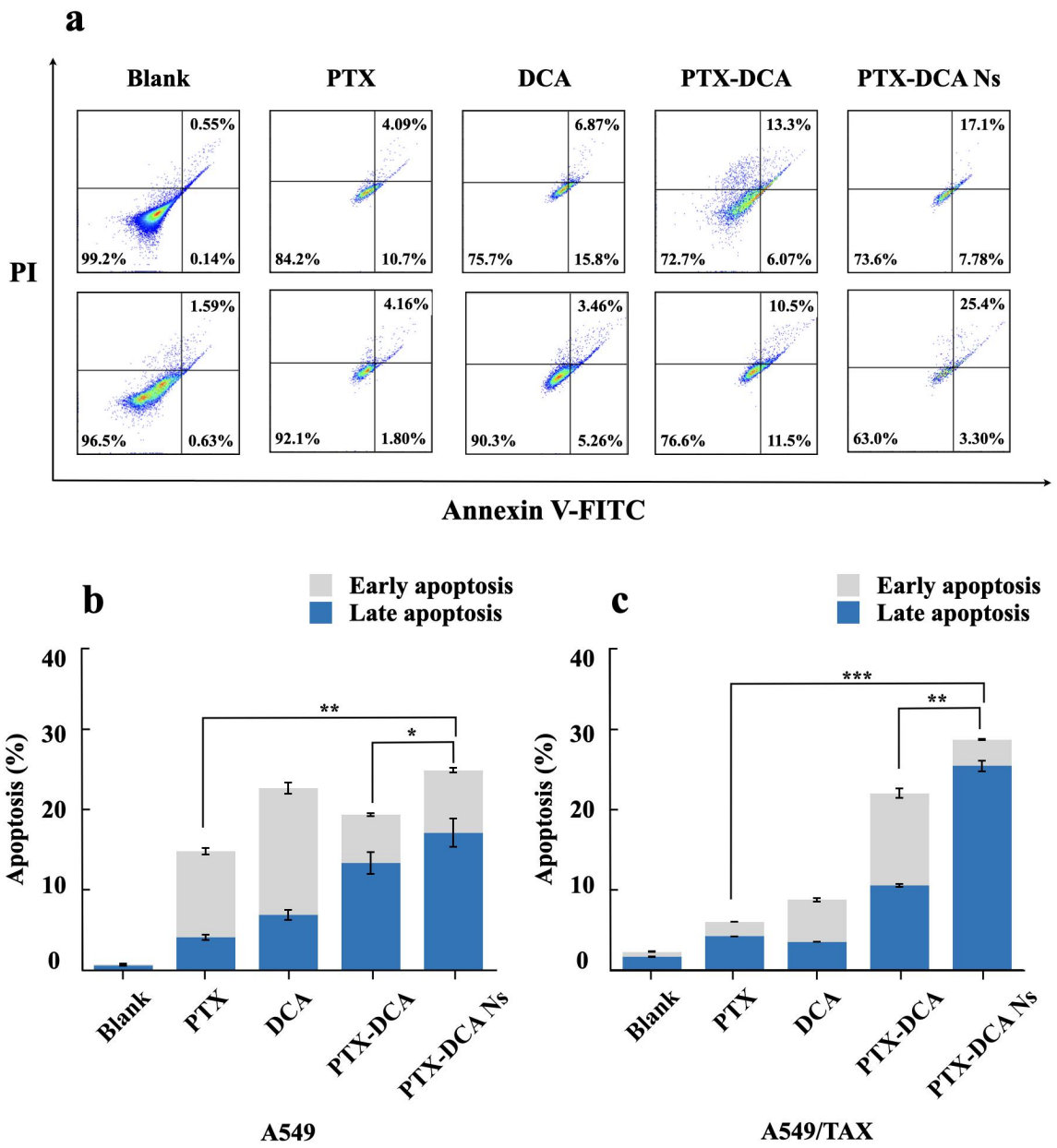

Figure 6 Apoptosis study. (a) Flow cytometric analysis for apoptosis in A549 (top) and A549/TAX (bottom) cells after treatment with different drug formulations at a PTX or DCA concentration of 50 μg/mL for 24 h at 37 °C. Quantified apoptosis assay in (b) A549 and (c) A549/TAX cells. $n = 3$, $^{*}P < 0.05$, $^{**}P < 0.01$, and $^{***}P < 0.001$

References

[1] J.M. Stewart, B.G. Keselowsky, Combinatorial drug delivery approaches for immunomodulation, Advanced Drug Delivery Reviews, 114 (2017) 161-174.
[2] W. He, X. Xing, X. Wang, D. Wu, W. Wu, J. Guo, S. Mitragotri, Nanocarrier-mediated cytosolic delivery of biopharmaceuticals, Advanced Functional Materials, 30 (2020) 1910566.
[3] K. Zhang, P.-P. Yang, J.-P. Zhang, L. Wang, H. Wang, Recent advances of transformable nanoparticles for theranostics, Chinese Chemical Letters, 28 (2017) 1808-1816.
[4] H. He, Y. Lu, J. Qi, Q. Zhu, Z. Chen, W. Wu, Adapting liposomes for oral drug delivery, Acta Pharmaceutica Sinica B, 9 (2019) 36-48.
[5] Y. Zhu, X. Yu, S.D. Thamphiwatana, Y. Zheng, Z. Pang, Nanomedicines modulating tumor immunosuppressive cells to enhance cancer immunotherapy, Acta Pharmaceutica Sinica B, 10 (2020) 2054-2074.
[6] I. Zoya, H. He, L. Wang, J. Qi, Y. Lu, W. Wu, The intragastrointestinal fate of paclitaxel-loaded micelles: Implications on oral drug delivery, Chinese Chemical Letters, (2020).
[7] C. Teng, C. Lin, F. Huang, X. Xing, S. Chen, L. Ye, H.S. Azevedo, C. Xu, Z. Wu, Z. Chen, W. He, Intracellular codelivery of anti-inflammatory drug and anti-miR 155 to treat inflammatory disease, Acta Pharmaceutica Sinica B, (2020).
[8] J. Li, D.J. Burgess, Nanomedicine-based drug delivery towards tumor biological and immunological microenvironment, Acta Pharmaceutica Sinica B, 10 (2020) 2110-2124.
[9] Y. Lu, Y. Li, W. Wu, Injected nanocrystals for targeted drug delivery, Acta Pharmaceutica Sinica B, 6 (2016) 106-113.
[10] R. Yang, T. Zhang, J. Yu, Y. Liu, Y. Wang, Z. He, *In vitro/vivo* assessment of praziquantel nanocrystals: Formulation, characterization, and pharmacokinetics in beagle dogs, Asian Journal of Pharmaceutical Sciences, 14 (2019) 321-328.
[11] Y. Lu, Y. Lv, T. Li, Hybrid drug nanocrystals, Advanced Drug Delivery Reviews, 143 (2019) 115-133.
[12] I.S. Mohammad, W. He, L. Yin, Smart Paclitaxel-Disulfiram Nanococrystals for Efficient MDR Reversal and Enhanced Apoptosis, Pharmaceutical Research, 35 (2018) 77.
[13] I.S. Mohammad, C. Teng, B. Chaurasiya, L. Yin, C. Wu, W. He, Drug-delivering-drug approach-based codelivery of paclitaxel and disulfiram for treating multidrug-resistant cancer, International Journal of Pharmaceutics, 557 (2019) 304-313.
[14] B. Kim, C. Lee, E.S. Lee, B.S. Shin, Y.S. Youn, Paclitaxel and curcumin co-bound albumin nanoparticles having antitumor potential to pancreatic cancer, Asian Journal of Pharmaceutical Sciences, 11 (2016) 708-714.
[15] D.R. Kohler, B.R. Goldspiel, Paclitaxel (Taxol), Pharmacotherapy: The Journal of Human Pharmacology and Drug Therapy, 14 (1994) 3-34.
[16] J.L. Roh, J.Y. Park, E.H. Kim, H.J. Jang, M. Kwon, Activation of mitochondrial oxidation by PDK2 inhibition reverses cisplatin resistance in head and neck cancer, Cancer Lett, 371 (2016) 20-29.
[17] F. Gong, X. Peng, Y. Sang, M. Qiu, C. Luo, Z. He, X. Zhao, A. Tong, Dichloroacetate induces protective autophagy in LoVo cells: involvement of cathepsin D/thioredoxin-like protein 1 and Akt-mTOR-mediated signaling, Cell Death & Disease, 4 (2013) e913-e913.
[18] I.A. Seliem, S.S. Panda, A.S. Girgis, Y.I. Nagy, R.F. George, W. Fayad, N.G. Fawzy, T.S. Ibrahim, A.M.M. Al-Mahmoudy, R. Sakhuja, Z.K.M. Abdel-samii, Design, synthesis, antimicrobial, and DNA gyrase inhibitory properties of fluoroquinolone–dichloroacetic acid hybrids, Chemical Biology & Drug Design, 95 (2020) 248-259.
[19] A. Kumar, S. Kant, S.M. Singh, Antitumor and chemosensitizing action of dichloroacetate implicates modulation of tumor microenvironment: a role of reorganized glucose metabolism, cell survival regulation and macrophage differentiation, Toxicol Appl Pharmacol, 273 (2013) 196-208.

[20] L. Zhou, L. Liu, W. Chai, T. Zhao, X. Jin, X. Guo, L. Han, C. Yuan, Dichloroacetic acid upregulates apoptosis of ovarian cancer cells by regulating mitochondrial function, Onco Targets Ther, 12 (2019) 1729-1739.
[21] R.K. Pathak, S. Marrache, D.A. Harn, S. Dhar, Mito-DCA: a mitochondria targeted molecular scaffold for efficacious delivery of metabolic modulator dichloroacetate, ACS Chem Biol, 9 (2014) 1178-1187.
[22] H. Wade, MD recognition by MDR gene regulators, Curr Opin Struct Biol, 20 (2010) 489-496.
[23] S.Y. Chen, S.S. Hu, Q. Dong, J.X. Cai, W.P. Zhang, J.Y. Sun, T.T. Wang, J. Xie, H.R. He, J.F. Xing, Establishment of Paclitaxel-resistant Breast Cancer Cell Line and Nude Mice Models, and Underlying Multidrug Resistance Mechanisms *in Vitro and in Vivo*, Asian Pac J Cancer Prev, 14 (2013): 6135-40
[24] N. Chadborn, J. Bryant, A.J. Bain, P. O'Shea, Ligand-dependent conformational equilibria of serum albumin revealed by tryptophan fluorescence quenching, Biophysical Journal, 76 (1999) 2198.
[25] G.H. Wu, J. Wang, J.L. Chen, C. Guo, P.S. Wang, D.X. Wang, Z.Q. Wang, Bovine serum albumin in the presence of zinc (II) by fluorescence method, Spectroscopy and Spectral Analysis, 28 (2008) 913-916.
[26] A. Toumadje, S.W. Alcorn, W.C. Johnson, Jr., Extending CD spectra of proteins to 168 nm improves the analysis for secondary structures, Anal Biochem, 200 (1992) 321-331.
[27] S.M. Kelly, T.J. Jess, N.C. Price, How to study proteins by circular dichroism, Biochim Biophys Acta, 1751 (2005) 119-139.
[28] K. Park, A. Perczel, G.D. Fasman, Differentiation between transmembrane helices and peripheral helices by the deconvolution of circular dichroism spectra of membrane proteins, Protein Sci, 1 (1992) 1032-1049.
[29] M.D. Hays, D.K. Ryan, S. Pennell, A modified multisite Stern-Volmer equation for the determination of conditional stability constants and ligand concentrations of soil fulvic acid with metal ions, Anal Chem, 76 (2004) 848-854.